Supporting Information for "Isotope ratio – discharge relationships of solutes derived from weathering reactions"

Jennifer L. Druhan* and Paolo Benettin†

This Supplemental Information material includes:

1. Text S1–S7
2. Figure S1–S5

Contents of this file

*Department of Geology, University of Illinois Urbana Champaign, Illinois, USA, and
Institut de Physique du Globe de Paris, Sorbonne Paris Cité, Université Paris Diderot, CNRS, Paris, France
†Laboratory of Ecohydrology ENAC/IIE/ECHO, École Polytechinque Fédérale de Lausanne (EPFL), Lausanne, Switzerland.

Text S1 Derivation of k_{eff} and C_{LIM}

Beginning with Eq. 1 in the main body of the paper, we choose to represent two reactive pathways with rate constants k_1 and k_2 and maximum concentrations C_{lim1} and C_{lim2}. Nominally, the first parameter set applies to a set of mineral-water reactions representing primary mineral dissolution, while the second parameter set applies to a set of secondary minerals than can form from soluton and potentially resolubilize:

$$\frac{dC}{dt} = k_1 \left(1 - \frac{C}{C_{\text{lim1}}}\right) + k_2 \left(1 - \frac{C}{C_{\text{lim2}}}\right) \tag{S1}$$

which can be expanded as

$$\frac{dC}{dt} = k_1 + k_2 - C \left(\frac{k_1}{C_{\text{lim1}}} + \frac{k_2}{C_{\text{lim2}}}\right) \tag{S2}$$

Applying separation of variables to the first order linear differential equation,

$$\frac{1}{k_1 + k_2} \frac{dC}{1 - AC} = dt \tag{S3}$$

where

$$A = \frac{1}{k_1 + k_2} \left(\frac{k_1}{C_{\text{lim1}}} + \frac{k_2}{C_{\text{lim2}}}\right) \tag{S4}$$

by allowing $u = 1 - AC$ such that $du = -AdC$, we can obtain the equality of integrals

$$\frac{1}{k_1 + k_2} \int -\frac{1}{A} \frac{du}{u} = \int dt \tag{S5}$$

Performing the integral,

$$-\frac{1}{A(k_1 + k_2)} (ln(u) + C) = t \tag{S6}$$

where C is a constant of integration that can be evaluated for the initial condition $C(0) = C_0$ to reach:

$$C(t) = \frac{1 - (1 - AC_0) exp(-A(k_1 + k_2)t)}{A} \tag{S7}$$

reinserting A (Eq. S4) yields an expanded form of the solution

$$C(t) = \frac{k_1 + k_2}{\frac{k_1}{C_{lim1}} + \frac{k_2}{C_l im2}} + \left(C_0 - \left(\frac{k_1 + k_2}{\frac{k_1}{C_{lim1}} + \frac{k_2}{C_l im2}}\right)\right) exp\left(-\left(\frac{k_1}{C_{lim1}} + \frac{k_2}{C_{lim2}}\right) t\right) \tag{S8}$$

which can be recast in a compact form using the following relationships:

$$C_{\text{LIM}} = \frac{k_1 + k_2}{k_1/C_{\text{lim1}} + k_2/C_{\text{lim2}}} \tag{S9}$$

$$k_{eff} = k_1 + k_2 \tag{S10}$$

to obtain Eq. 2 in the main body of text:

$$C(t) = C_{\text{LIM}} + (C_0 - C_{\text{LIM}}) \exp\left(-\frac{k_{eff}}{C_{LIM}} t\right) \tag{S11}$$

Text S2 The Water Age Balance Equation

The water age balance formulated in terms of rank storage (S_T) reads (Harman, 2015; Benettin & Bertuzzo, 2018):

$$\frac{\partial S_T(T,t)}{\partial t} + \frac{\partial S_T(T,t)}{\partial T} = J(t) - Q(t)\,\Omega_Q(S_T(T,t),t) \tag{S12}$$

with Initial Condition $S_T(T, t = 0) = S_{T_0}$ and Boundary Condition $S_T(T = 0, t) = 0$. In Equation (S12), J is rainfall, Q is streamflow, T is age, t is time and $\Omega_Q(S_T, t)$ is the StorAge Selection (SAS) function for streamflow. The equation is solved by using the method of characteristics and a Euler Forward discretization (see Benettin & Bertuzzo, 2018). The hydrologic fluxes in Equation (S12) are shown in section Text S6 and the SAS function parameterization is presented in the main text.

Text S3 Recovery of Rayleigh distillation under simplifying conditions

Here we illustrate recovery of Rayleigh distillation in our model framework under the simplifying condition that the dissolution of primary minerals are entirely omitted, and instead we use an initial condition that is oversaturated with respect to C_{lim2}, e.g $C_0/C_{lim2} = 4.0$ (Figure S1). In this case, the $SiO_{2(aq)}$ concentration decreases through time, and eventually reaches C_{lim2}, at which point the reaction has reached completion. Using a fractionation factor of $\alpha_2 = 0.998$, the resulting evolution in fluid $\delta^{30}Si$ produces classic Rayleigh distillation in the approach to C_{lim2}.

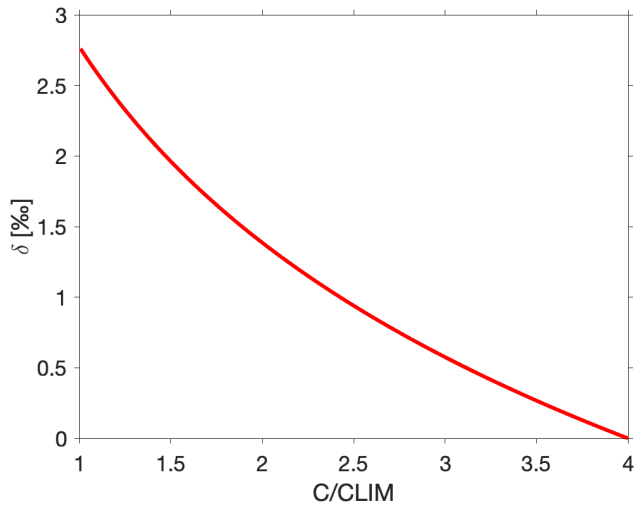

Figure S1: Demonstration of isotopic fractionation in a system subject only to clay precipitation (no primary mineral dissolution) and starting from an initially oversaturated fluid $SiO_{2(aq)}$ value such that $C_0/C_{lim2} = 4.0$. As the reaction proceeds to completion, $C \rightarrow C_{LIM}$ and the model returns classic Rayleigh distillation.

Text S4 Constraint of solubility limits from CrunchFlow multi-component model

We first extract the assemblage of primary minerals used in the CrunchFlow model for the Santa Cruz chronosquence (Maher, Steefel, White, & Stonestrom, 2009; Lawrence, Harden, & Maher, 2014; Druhan & Lawrence, 2021), which include a potassium feldspar:

$$KAlSi_3O_8 \rightarrow K^+ + AlO_2^- + 3SiO_{2(aq)} \tag{S13}$$

as well as an albite-anorthite solid solution:

$$Na_{0.9}Ca_{0.1}Al_{1.1}Si_{2.9}O_8 \rightarrow 0.9Na^+ + 1.1AlO_2^- + 0.1Ca^{++} + 2.9SiO_{2(aq)} \tag{S14}$$

we use the same rate laws for these minerals given in Maher et al. (2009) with rate constant of $10^{-14.9} mol/m^2 - s$ and starting surface areas of 1.14 and 1.94 m^2/g, respectively, and simply allow these reactions to proceed to completion in the absence of any fluid flow or solute transport. From this result we extract a maximum $SiO_{2(aq)}$ concentration of 800 uM for a temperature of 13.5°C.

Next, these primary minerals are removed and replaced by kaolinite, again following the stoichiometry given by Maher et al. (2009):

$$Al_2Si_2O_5(OH)_4 + 8H^+ \leftrightarrow 2Al^{3+} + 2SiO_{2(aq)} + 5H_2O \tag{S15}$$

following a reversible rate law with rate constant of $10^{-19.8} mol/m^2 - s$ and starting surface areas of 10 m^2/g. The result is a maximum $SiO_{2(aq)}$ concentration of 150 uM for a temperature of 13.5°C.

All mineral volume fractions and starting solute concentrations as reported in Maher et al. (2009) and Lawrence et al. (2014). Importantly, the kinetic parameters and mineral surface areas used in these prior models are only indirectly incorporated into the present study in that the balance of individual mineral weathering rates for Eq. (S13 & S14) contributes to the final steady state concentration of $SiO_{2(aq)}$. Essentially we rely on the rigorous thermodynamics and stoichiometry developed in these prior models to produce appropriate values of C_{lim} for our present purposes and proceed by utilizing these values in combination with an appropriate representation of R_p/R_d.

Text S5 Geochemical model evolution to steady state

Here we demonstrate the behavior of the silicate weathering model described in sections (2.2–2.3) in a simplified system in which fluid $SiO_{2(aq)}$ concentrations are allowed to evolve from an initial value of zero to a final steady state C_{LIM} value through time (Figure S2A). Rate constants of $k_1 = 1$ µM/d and $k_2 = 0.5$ µM/d yield an $R_p/R_d = 0.5$ and result in a $C_{LIM} = 327$ µM. In comparison, adjusting k_2 to allow for an $R_p/R_d = 1.0$ essentially speeds up the rate of clay formation, resulting in a lower C_{LIM} value that reaches steady state faster. Alternatively, an $R_p/R_d = 0.25$ slows down the clay formation rate, creating a larger C_{LIM} that takes longer to stabilize. All three of these simulations use the same fixed values of C_{lim1} and C_{lim2}, highlighting the dynamic

nature of the effective C_{LIM} that may be established through the balance in these two components of the overall reaction rate.

As noted in the main text (section 2.3) an $R_p/R_d = 0.5$ was suggested as an appropriate ratio for $SiO_{2(aq)}$ during contemporaneous weathering of feldspars and accumulation of kaolinites by (Maher, 2011). Using this ratio and our specific values of k_1 and k_2, we are able to achieve close agreement with the comparable model for $SiO_{2(aq)}$ developed by Maher (2011, 2010) in the absence of any fluid residence time distributions.

For parameters appropriate to describe $\delta^{30}Si$ partitioning during silicate weathering (Table 1) the model achieves an enrichment in the fluid phase on the order of 1.2‰ as the system reaches steady state for an $R_p/R_d = 0.5$ (Figure S2B). A larger R_p/R_d value drives more clay precipitation relative to primary mineral dissolution, and hence achieves a larger enrichment, whereas the opposite effect is observed for a lower R_p/R_d ratio. The subtle behavior at early time noted in the main text is clearly illustrated here, specifically before the fluid $SiO_{2(aq)}$ concentration has crossed the C_{lim2} threshold.

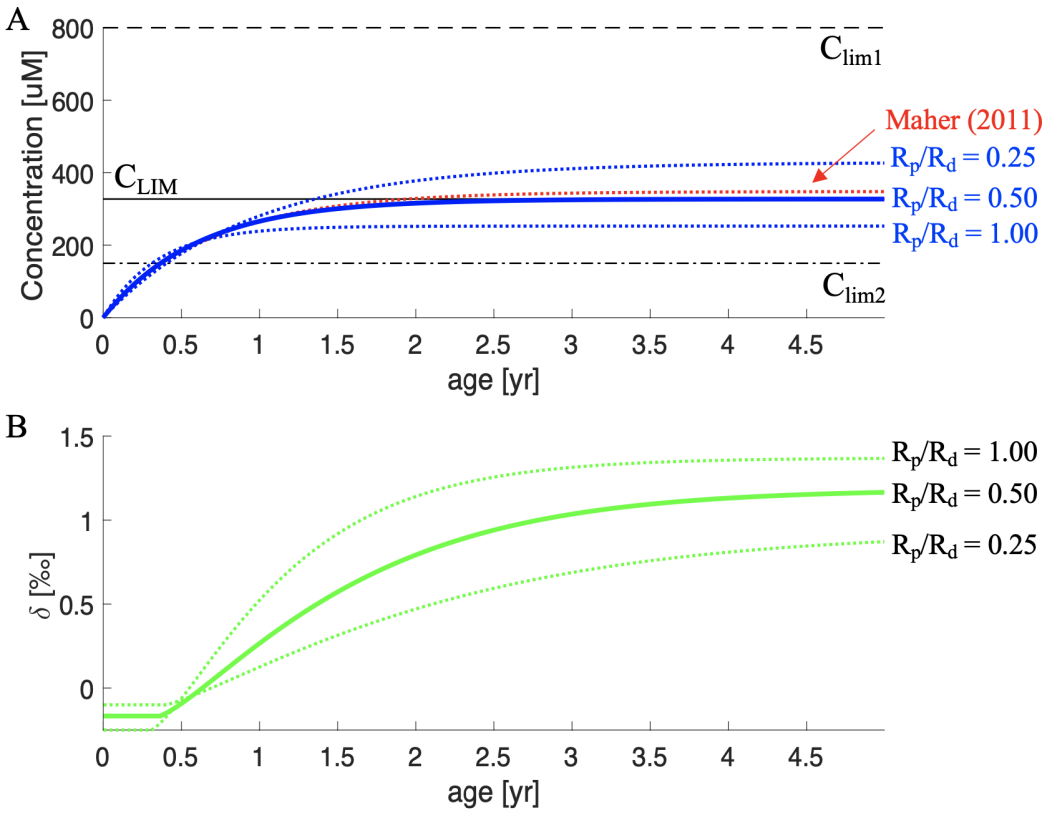

Figure S2: (A) Application of Eq. 12–13 in a closed system advancing through time from an initial condition of zero $SiO_{2(aq)}$ using parameter values given in section 2.3. The initial increase in $SiO_{2(aq)}$ is due to dissolution of both group 1 ($k_1(1 - C/C_{lim1})$) and group 2 ($k_2(1 - C/C_{lim2})$) components of the reaction rate. After approximately 140 days the C_{lim2} threshold is exceeded and this component of the reaction rate begins to remove $SiO_{2(aq)}$ from solution, ultimately establishing a steady state C_{LIM} of 327 uM. Close agreement is noted between the simulation using an $R_p/R_d = 0.5$ and the model developed by Maher (2011, 2010). Two alternate values of R_p/R_d are illustrated by adjustment of the k_2 rate constant. (B) Corresponding aqueous δ^{30}Si time series is also shown.

Text S6 Hydrologic time series

The hydrologic used to develop and test the model were generated numerically. The virtual timeseries lasts 2 years and it was repeated 4 times for the simulations (where the first 6 years were used as spinup). Rainfall was generated as a Poisson process with annual rainfall depth of 1200 mm and mean inter-arrival of 10 days. No evapotranspiration or deep losses are considered and all rainfall eventually forms runoff. Streamflow was generated using a series of 2 non-linear bucket models (see e.g. Kirchner, 2016) of the type:

$$Q_i(t) = a_i \left(\frac{S_i(t)}{S_{max_i}} \right)^{b_i} \tag{S16}$$

where i denotes either of the two buckets, $Q_i(t)$ and $S_i(t)$ are the outflow and storage of the bucket, respectively, and a_i, S_{max_i} and b_i are parameters. Additionally, a parameter f_p regulates the fraction of outflow that goes from one bucket to the next. By changing these parameters, one can get a large range of different hydrologic behaviors. We selected the parameters such that one bucket had a more reactive, smaller storage (and we interpret this bucket as a soil water storage), while the other had a slower and larger storage (and we interpret it as a shallow groundwater storage). Through the combination of these two runoff components, the simulated streamflow responds quickly to rainfall events (mainly due to soil water contributions) but flow is sustained during dry periods (thanks to the slower and more persistent groundwater contributions). The ratio between soil water and groundwater flow contributions is termed w in the main paper and it is used to control the temporal variability of the SAS function. Timeseries of J, Q and w are shown in Figure S3.

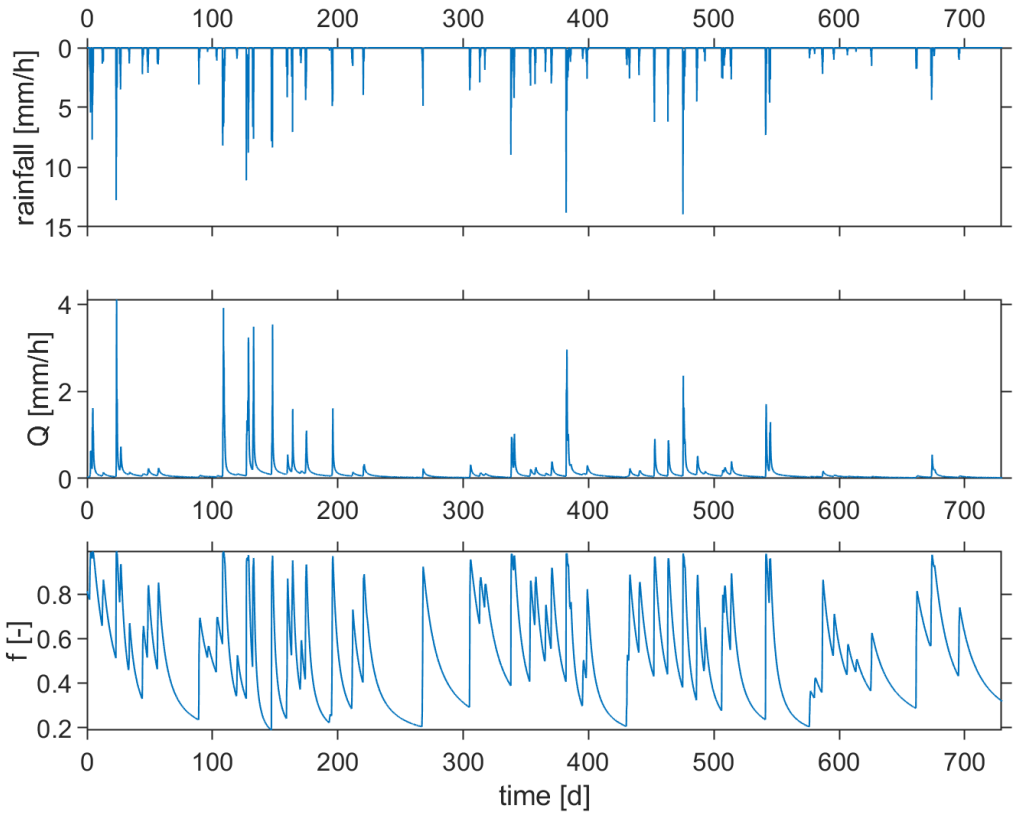

Figure S3: Timeseries of the virtual hydrologic fluxes used in the simulations. Top: rainfall (J), middle: streamflow (Q), bottom: ratio soil to groundwater contribution (w) used to control the variability in the SAS function shape.

Text S7 Additional supplementary figures

Additional supplementary figures S4–S5 are shown below.

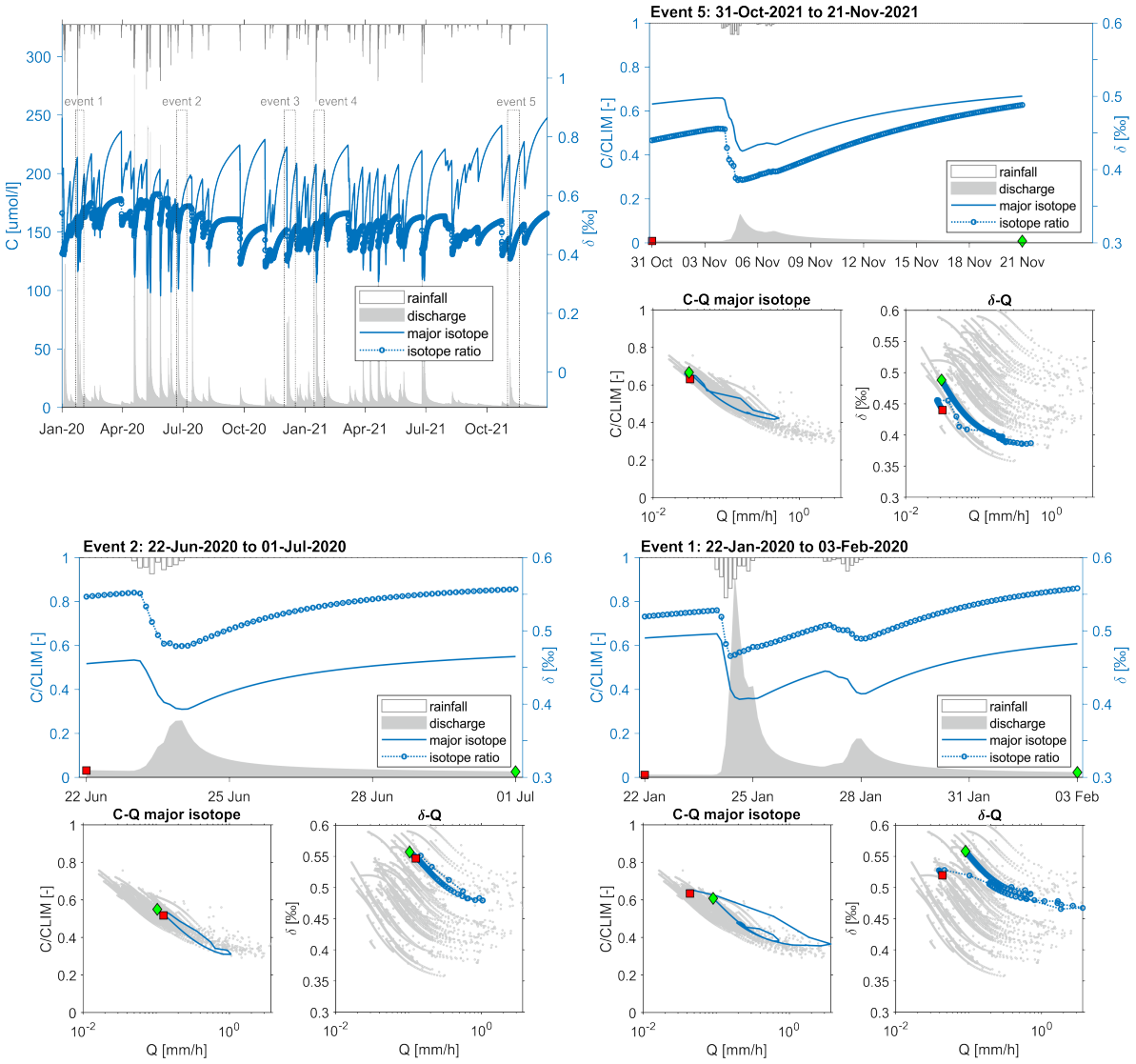

Figure S4: Selected hydrologic events 1,2 and 5. The figure on the top-left shows the full 2-year timeseries and marks 5 different events. Events 3–4 are reported and discussed in the main paper.

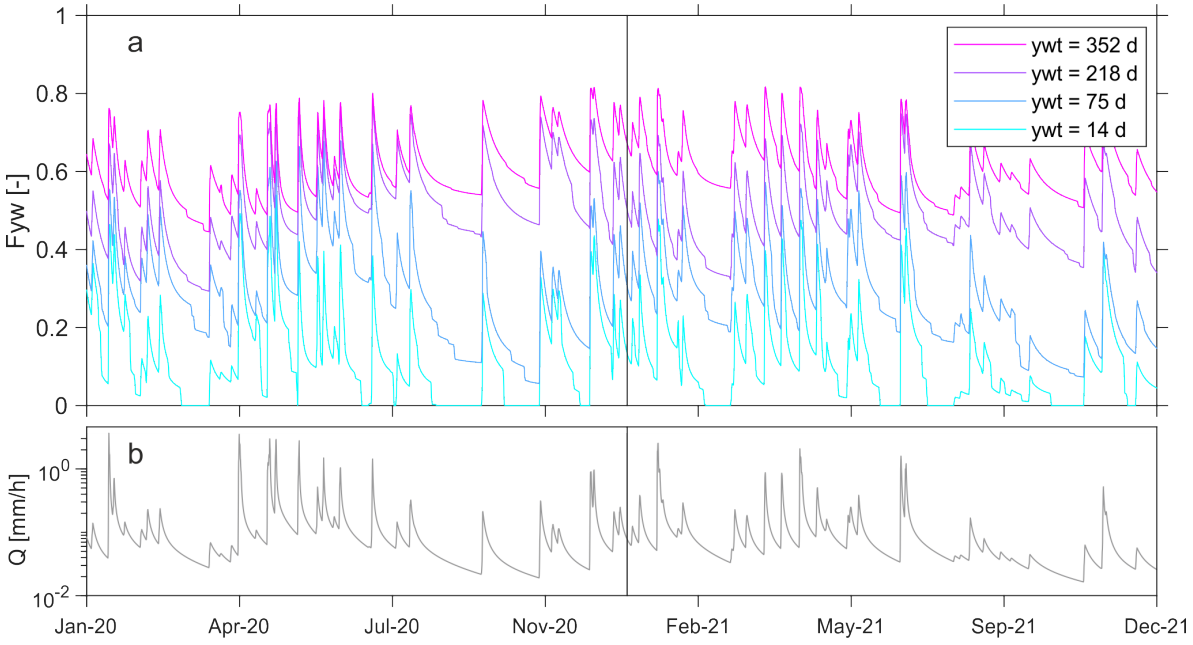

Figure S5: Timeseries of four definitions of F_{yw}. These timeseries are strongly correlated to streamflow and to each other. The youngest fraction (corresponding to $y_{wt} = 14$ days) is more irregular and occasionally null because the availability of water younger than 14 days depends on the erratic cycles of precipitation. The curves are less variable for older fractions and approximately 60% of streamflow is made of water younger than 1 year.

References

Benettin, P., & Bertuzzo, E. (2018). tran-SAS v1. 0: a numerical model to compute catchment-scale hydrologic transport using StorAge selection functions. *Geoscientific Model Development*, *11*(4), 1627–1639. doi: doi:10.5194/gmd-11-1627-2018

Druhan, J. L., & Lawrence, C. R. (2021). Development of soil radiocarbon profiles in a reactive transport framework. *Geochimica et Cosmochimica Acta*, *306*, 63–83.

Harman, C. J. (2015). Time-variable transit time distributions and transport: Theory and application to storage-dependent transport of chloride in a watershed. *Water Resources Research*, *51*(1), 1–30. doi: doi:10.1002/2014WR015707

Kirchner, J. W. (2016). Aggregation in environmental systems - Part 2: Catchment mean transit times and young water fractions under hydrologic nonstationarity. *Hydrology and Earth System Sciences*, *20*(1), 299–328. doi: doi:10.5194/hess-20-299-2016

Lawrence, C., Harden, J., & Maher, K. (2014). Modeling the influence of organic acids on soil weathering. *Geochimica et Cosmochimica Acta*, *139*, 487–507.

Maher, K. (2010). The dependence of chemical weathering rates on fluid residence time. *Earth and Planetary Science Letters*, *294*(1–2), 101–110. doi: doi:10.1016/j.epsl.2010.03.010

Maher, K. (2011). The role of fluid residence time and topographic scales in determining chemical fluxes from landscapes. *Earth and Planetary Science Letters*, *312*, 48–58. doi: doi:10.1016/j.epsl.2011.09.040

Maher, K., Steefel, C. I., White, A. F., & Stonestrom, D. A. (2009). The role of reaction affinity and secondary minerals in regulating chemical weathering rates at the santa cruz soil chronosequence, california. *Geochimica et Cosmochimica Acta*, *73*(10), 2804–2831.